Advances in Applied Mathematics and Mechanics
Adv. Appl. Math. Mech., Vol. **xx**, No. x, pp. 1-20

DOI: 10.4208/aamm.OA-2021-0220
xxx 2022

# Interaction of Radiation and Turbulent Natural Convection: A Pseudo-Direct Numerical Study

Alexander Nee[1,*] and Ali J. Chamkha[2]

[1] *Research and Educational Center of I.N. Butakov, National Research Tomsk Polytechnic University, Tomsk, Russia*
[2] *Faculty of Engineering, Kuwait College of Science and Technology, Doha District, Kuwait*

Received 29 June 2021; Accepted (in revised version) 3 February 2022

**Abstract.** This paper presents a hybrid lattice Boltzmann solver for turbulent buoyancy-driven flow coupled with surface thermal radiation. The two-relaxation time scheme for the Boltzmann equation combined with the implicit finite difference scheme for the energy equation is implemented to compute the heat transfer and fluid flow characteristics. The accuracy and robustness of the hybrid approach proposed in this study are assessed in terms of the numerical and experimental data of other researchers. Upon performing the simulation, the Rayleigh number is ranged from 108 to 1010 whereas the surface emissivity is changed from zero to unity. During computations, it is found that the overall temperature of the cavity is increased as a result of enhancing the surface radiation. Convective plumes are formed both at the isothermal and the thermally-insulated walls with the $Ra \geq 10^9$ and $\varepsilon \geq 0.6$. In the conditions under study, the overall heat transfer rate is raised by around 5% when taking into account the surface thermal radiation.

**AMS subject classifications**: 80A20, 76F65

**Key words**: Pseudo-direct numerical simulation, surface radiation, hybrid lattice Boltzmann scheme, turbulent natural convection.

## 1 Introduction

Turbulent natural convective mechanism of heat transfer is encountered in many practical applications such as building heating, fuel cells cooling, metal industry, etc. Despite a significant development of computational fluid dynamics tools, an accurate prediction of turbulent flow behavior is still a very complicated task since a conventional direct

*Corresponding author.
*Emails:* nee_alexander@mail.ru (A. Nee), a.chamkha@kcst.edu.kw (A. Chamkha)

 

numerical simulation (DNS) approach is computationally inefficient. Moreover, numerical implementation becomes much more difficult when taking into account the radiative heat transfer [1]. Based on the literature review, the works devoted to the combined heat transfer by turbulent natural convection and radiation can be classified by the turbulence model used. Below, the up-to-date works will be discussed.

As could be expected, mathematical modelling predominantly performed in terms of the Reynolds averaged Navier-Stokes (RANS) approach. The popularity of the RANS is due to acceptable time of code execution. However, it should be stressed that this approach contains several empirical constants. Sharma and co-workers considered turbulent buoyancy driven flow in rectangular [2] and inclined square [3] enclosures filled with a transparent medium when taking into account the surface radiation. Turbulent natural convection was computed in terms of the standard kinetic energy and its dissipation rate ($k-\varepsilon$) model. The effect of walls emissivity on turbulent buoyancy driven flow of the humid air in a cavity with cylindrical obstacles was analyzed by Iyi et al. [4]. Heat transfer via turbulent natural convection and surface thermal radiation in an enclosure partially filled with a porous medium was studied in [5]. Dash and Dash [6] considered turbulent natural convection from a hot horizontal cylinder. The radiation transport equation was solved by means of the discrete ordinate method. Parmananda et al. [7] examined the effect of non-Boussinesq formulation on turbulent heat transfer and fluid flow characteristics. A low Mach number model was utilized to perform numerical study. Xaman et al. [8, 9] analyzed the turbulent buoyancy flow coupled with the conjugate heat transfer and surface radiation. These studies were aimed to find out how a vertical glazed wall affected the thermal and flow behavior. Sheremet et al. [10, 11] considered the same heat transfer modes in a cavity bounded by solid walls with a discrete heater. Moreover, the authors implemented the standard $k-\varepsilon$ model with a coordinate transformation in order to perform computations on a non-uniform mesh.

While the studies [2–11] implemented the $k-\varepsilon$ model, Zamora and Kaiser [12–14] performed computations with the standard kinetic energy and its specific dissipation rate ($k-\omega$) model. They considered the effect of temperature-dependent physical properties, cavity shape and the presence of a hot immersed body on local and mean fluid dynamics characteristics. Radiation was described by means of the IMMERSOL model. Hemmer et al. [15] studied thermal and flow fields in a room with convective and radiant heaters. The shear stress transport (SST) $k-\omega$ model of Menter was applied to calculate turbulent fluxes. The same turbulence model was used to analyze the effect of aspect ratio [16] on the flow structure and electronics cooling characteristics [17]. Comparative studies of performance of different $k-\varepsilon$ and $k-\omega$ models in combined heat transfer problems by turbulent natural convection and radiation are discussed in [18–20].

By now, few papers analyze the turbulent buoyancy driven flows coupled with radiation in terms of the LES and DNS techniques. Kogawa et al. [21] built a complex three-dimensional model to analyze how the non-radiation, surface radiation, volumetric radiation and combined radiation affected the heat transfer and turbulent fluid flow patterns. The large eddy simulation coupled with the dynamic Vreman subgrid model

was used in their study. On the other hand, Xin et al. [22] performed direct numerical simulation of turbulent natural convection combined with conduction and surface radiation. Spectral methods were applied as a fluid dynamics solver. The Rayleigh number of $Ra = 1.5 \times 10^9$ was set for all computations.

The studies presented above reflect the current state of the problem under consideration. During literature review, it was found that numerical simulation of turbulent natural convection coupled with radiation were conducted in terms of the Reynolds averaged Navier-Stokes method. However, it should be stressed that this method lacks accuracy and significantly overpredicts the heat transfer rate when analyzing natural convection in a closed cavity [23]. On the other hand, a little attention is paid to direct numerical simulation since this approach is still computationally expensive. In order to fill the gap in this research area, a hybrid lattice Boltzmann model is developed. The motivation of this study is to examine the heat transfer and high Rayleigh number fluid flow patterns when taking into account the surface thermal radiation by means of the pseudo-DNS technique.

## 2 Problem description

Pseudo-direct or quasi-direct numerical simulation (pDNS) is a computational fluid dynamics approach for turbulence modeling. This approach is similar to conventional direct numerical simulation (DNS) technique. The difference between the pDNS [24,25] and the DNS is in computational grid resolution. The Kolmogorov scales of time and space are always resolved under the DNS method whereas these scales can be partially unresolved under the pDNS technique. It needs to be noted that numerical viscosity imitates physical dissipation within pseudo-direct numerical simulation approach. Hence, the choice of appropriate finite difference schemes along with an appropriate validation is crucial under the pDNS method.

The geometrical model of the thermal boundary value problem under study is presented in Fig. 1. The physical model assumed that the thermal diffusivity, heat conductivity and viscosity of the fluid are independent of temperature. The vertical walls are isothermal and the horizontal boundaries are assumed to be thermally-insulated. Transient Newtonian flow of a radiatively-transparent fluid is considered in two dimensions. The no-slip condition is set at the solid walls. Along with that, the boundaries are assumed diffusive and grey. Surface radiation is taken into account.

### 2.1 Turbulent buoyancy driven flow solver

In order to simulate the high Rayleigh number flow, the Boltzmann equation is used:

$$\frac{\partial f}{\partial t} + u \cdot \nabla f = \Omega. \tag{2.1}$$

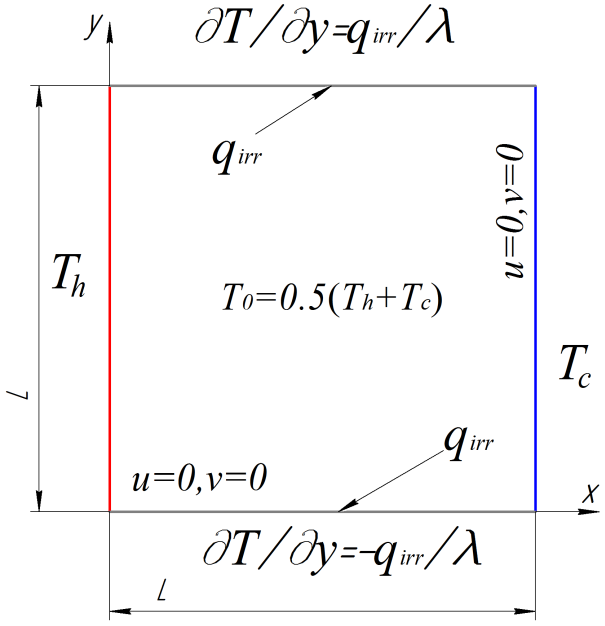


Figure 1: Analysis domain.

It is well-known that the wide-spread Bhatnagar-Gross-Krook approximation [26] suffers from numerical instabilities when setting the Rayleigh number higher than $10^8$. Hence, to overcome this weakness, a two-relaxation time (TRT) approximation [27, 28] coupled with the two-dimensional nine-velocity (D2Q9) scheme is implemented:

$$f_k(\vec{x}+\vec{c}_k\cdot\Delta t,t+\Delta t)=f_k(\vec{x},t)-\Delta t\cdot\omega_s\cdot\left(f_k^s-f_k^{seq}\right)-\Delta t\cdot\omega_a\cdot\left(f_k^a-f_k^{aeq}\right)+\Delta t\cdot F, \tag{2.2}$$

In Eq. (2.2) the $f_k^s$ is a symmetrical part of distribution function whereas $f_k^a$ is an asymmetrical one. The subscript $-k$ shows the inverse movement of $k$ (Fig. 2).

The equilibrium state of the distribution function is expressed as:

$$f_k^{eq}=w_k\cdot\rho\cdot\left[1+\frac{c_k\cdot u}{c_s^2}+\frac{(c_k\cdot u)^2}{2\cdot c_s^4}-\frac{u^2}{2\cdot c_s^2}\right]. \tag{2.3}$$

The weights for the two-dimensional nine-velocity scheme are $w_1=4/9$, $w_{2\sim5}=1/9$, $w_{6\sim9}=1/36$.

The following expressions are used to compute the macroscopic characteristics of fluid:

$$\rho=\sum_{k=1}^{9}f_k, \tag{2.4a}$$

$$u=\frac{1}{\rho}\cdot\sum_{k=1}^{9}c_k\cdot f_k. \tag{2.4b}$$

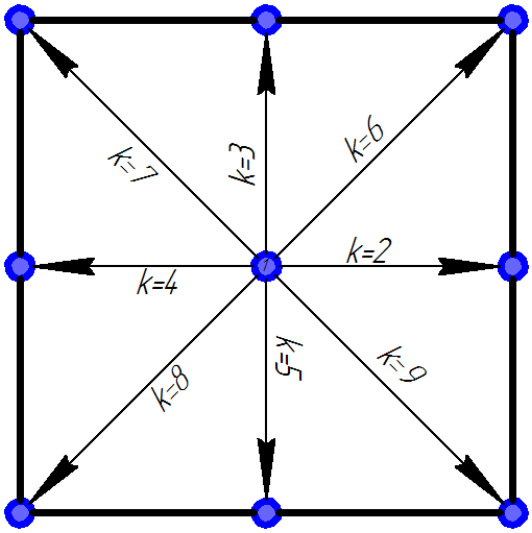


Figure 2: D2Q9 scheme.

The symmetrical relaxation rate is related to the kinematic viscosity as:

$$\omega_s = \frac{1}{3\cdot\nu+0.5}. \tag{2.5}$$

The coupling between symmetrical and asymmetrical relaxation rates is established through a "magic" parameter as [29,30]:

$$\Lambda = \left(\frac{1}{\omega_s}-0.5\right)\cdot\left(\frac{1}{\omega_a}-0.5\right). \tag{2.6}$$

In the present study, the "magic" parameter is set $1/4$ in order to maintain the highest numerical stability. Hence, the asymmetrical relaxation rate was computed as:

$$\omega_a = 2-\omega_s. \tag{2.7}$$

The natural convective effects are taken into account in the force term as:

$$F = 3\cdot\rho\cdot w_k\cdot c_y\cdot g\cdot\beta\cdot(T-T_0). \tag{2.8}$$

A simple boundary condition of the so-called bounce back is applied to compute the $f_k$ at the walls.

## 2.2 Heat transfer solver

In order to achieve the higher numerical stability, the passive scalar approach commonly used is swapped to a hybrid thermal model [31–33]. Within the hybrid formulation,

the advection/diffusion equation is solved by means of the conventional computational fluid dynamics technique instead of additional lattice Boltzmann equation for temperature/concentration.

The two-dimensional energy equation without internal heat generation is as follows:

$$\frac{\partial T}{\partial t}+u\frac{\partial T}{\partial x}+v\frac{\partial T}{\partial y}=a\left(\frac{\partial^2 T}{\partial x^2}+\frac{\partial^2 T}{\partial y^2}\right). \tag{2.9}$$

The following boundary conditions are set:

- at the left wall:

$$T=T_h. \tag{2.10}$$

- at the right wall:

$$T=T_c. \tag{2.11}$$

- at the bottom and top walls:

$$\lambda\frac{\partial T}{\partial Y}\pm q_{irr}=0. \tag{2.12}$$

In order to find the irradiation in Eq. (2.12), firstly, the radiosity is computed as:

$$q_{rad,i}=\varepsilon_i\cdot\sigma\cdot T_i^4+(1-\varepsilon_i)\cdot\sum_{j=1}^{N}\left(q_{rad,j}\cdot\varphi_{i-j}\right). \tag{2.13}$$

The radiosity and irradiation are related as:

$$q_{irr,i}=q_{rad,i}-\sum_{j=1}^{N}\varphi_{i-j}\cdot q_{rad,j}. \tag{2.14}$$

When applying the following relationships

$$X=\frac{x}{L},\quad Y=\frac{y}{L},\quad U=\frac{u}{V_{nc}},\quad V=\frac{v}{V_{nc}},$$
$$V_{nc}=\sqrt{g\cdot\beta\cdot(T_h-T_c)\cdot L},\quad \Theta=\frac{T-T_c}{T_h-T_c},\quad Q_{rad}=\frac{q_{rad}}{\sigma\cdot T_h^4},\quad Q_{irr}=\frac{q_{irr}}{\sigma\cdot T_h^4},$$
$$\tau=\frac{t}{t_0},\quad t_0=\frac{L}{V_{nc}},\quad N_r=\frac{\sigma\cdot {T_h}^4\cdot L}{\lambda\cdot(T_h-T_c)},\quad Pr=\frac{\nu}{a},\quad Ra=\frac{g\cdot\beta\cdot(T_h-T_c)\cdot L^3}{\nu\cdot a}.$$

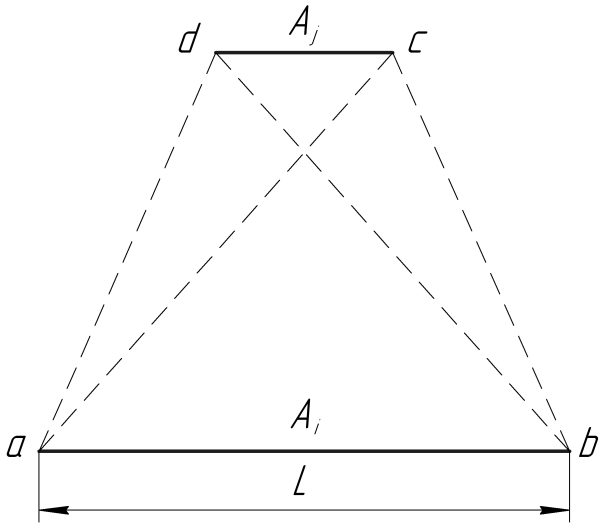


Figure 3: View factor calculation.

Eqs. (2.8)-(2.14) take the non-dimensional form which is more convenient for overall analysis. The dimensionless heat transfer model is as follows:

$$\frac{\partial\Theta}{\partial\tau}+U\frac{\partial\Theta}{\partial X}+V\frac{\partial\Theta}{\partial Y}=\frac{1}{\sqrt{Ra\cdot Pr}}\left(\frac{\partial^2\Theta}{\partial X^2}+\frac{\partial^2\Theta}{\partial Y^2}\right), \tag{2.15a}$$

$$X=0,\quad 0<Y<1:\quad \Theta=\Theta_h, \tag{2.15b}$$

$$X=1,\quad 0<Y<1:\quad \Theta=\Theta_c, \tag{2.15c}$$

$$\frac{\partial\Theta}{\partial Y}\pm N_r\cdot Q_{irr}=0, \tag{2.15d}$$

$$Q_{rad,i}=\varepsilon_i\cdot{\Theta_i}^4+(1-\varepsilon_i)\cdot\sum_{j=1}^{N}\varphi_{i-j}\cdot Q_{rad,j}, \tag{2.15e}$$

$$Q_{irr,_i}=Q_{rad,i}-\sum_{j=1}^{N}\varphi_{i-j}\cdot Q_{rad,j}, \tag{2.15f}$$

where $Ra$ is the Rayleigh number, $Pr$ is the Prandtl number, $Nr$ is the conduction-radiation number. It should be noted that the view factors were computed be means of the cross string method for two-dimensional geometries (Fig. 3).

In accordance with this method, a view factor between two surfaces is calculated as:

$$\varphi_{A_i-A_j}=\frac{1}{2\cdot L}\left[\left(\overline{ac}+\overline{bd}\right)-\left(\overline{ad}+\overline{bc}\right)\right].$$

The governing heat transfer equation along with the boundary conditions is discretized by the finite difference technique. The two-dimensional energy equation is approximated

by the implicit locally one-dimensional scheme of Samarskii. In order to discretize convective terms, the second-order monotonic Samarskii scheme is used. The system of linear algebraic equations with tridiagonal matrix obtained after discretization is solved by means of the Thomas algorithm. More details on numerical procedure can be found in the previous works [29,30].

### 2.3 Validation

In order to solve the governing equations, an in-house code is written in MATLAB R2017a. This code is tested on several benchmark problems. Firstly, numerical [36] and experimental [37] data obtained for the case of pure turbulent natural convection are compared. As could be seen from Fig. 4, both the temperature and Nusselt numbers are in a very good agreement with the data of Sharma et al. [36], Ampofo and Karayanis [37]. However, an increment in the error is observed as the Rayleigh number is increased. But still, an overall divergence is within 5%.

To verify the radiosity-irradiation model, laminar natural convection coupled with surface radiation in an air-filled cavity is considered. Fig. 5 shows the dimensionless temperature and the velocity profiles in the section of $=0.5$.

When analyzing the data presented in Fig. 5, a satisfactory agreement is observed with the benchmark data of Wang et al. [38]. Hence, the in-house code developed in this study is successfully verified.

It needs to be stressed that the grid sensitivity analysis under pseudo-direct numerical simulation technique is a non-trivial issue. On the one hand, a relatively coarse grid in comparison with pure DNS method can be implemented. On the other hand, numerical results can be drastically altered when the grid size is increased. Hence, grid-dependence test should be performed. The results are presented in Table 1.

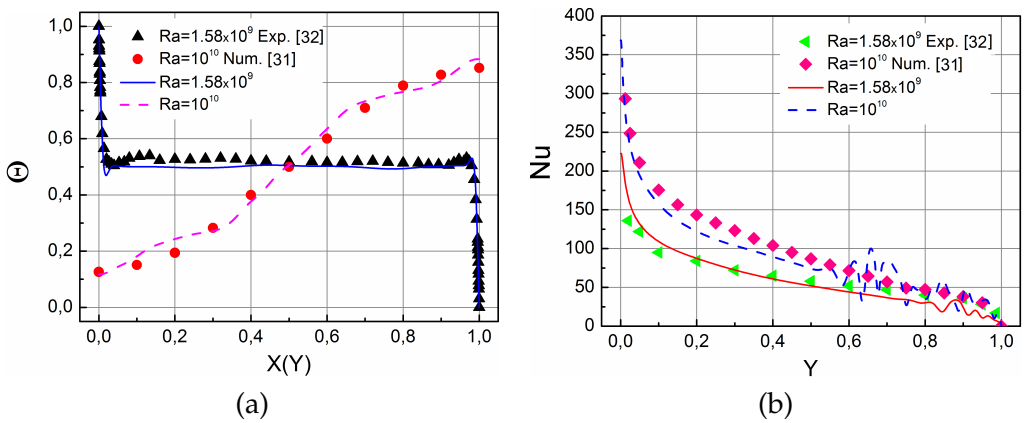


Figure 4: Variation of temperature (a) in the characteristic sections and local Nusselt number (b) at the hot wall.

Table 1: Variation of mean Nusselt numbers with the grid size when $Ra=10^9$, $Pr=0.71$, $N_r=300$ and $\varepsilon=0.5$.

| Grid | $501^2$ | $601^2$ | $701^2$ | $801^2$ |
|---|---|---|---|---|
| $Nu_C$ | 79.02 | 84.18 | 89.29 | 89.18 |
| $Nu_R$ | 4.74 | 4.75 | 4.75 | 4.74 |
| $Nu_E$ | 83.76 | 88.93 | 94.04 | 93.91 |

When analyzing the data presented in Table 1, it is observed that the grid size affects the mean convective and effective Nusselt numbers. On the contrary, the mean radiative Nusselt number is slightly changed with an increase in the mesh points. This behavior is predictable since the isothermal and adiabatic boundaries are considered. The sum up, a relative error does not exceed 0.15% between the grid sizes of $701^2$ and $801^2$. Hence, a uniform mesh of $701^2$ points provides grid-independent results.

## 3 Results and discussion

Turbulent free convection coupled with surface radiation was studied in a fluid-filled enclosure with the Pr of 0.71. The main attention was focused on the effect of the walls emissivity and value of buoyancy force on thermal and flow behavior. The $Ra$ was varied in a range of $10^8 \leq Ra \leq 10^{10}$ whereas the Nr was ranged in $75.89 \leq N_r \leq 351.75$. Emissivity of the walls was changed from zero to unity. The data computed during simulations are presented in terms of the temperature contours, velocity streamslices, temperature and velocity profiles, convective, radiative and effective Nusselt numbers.

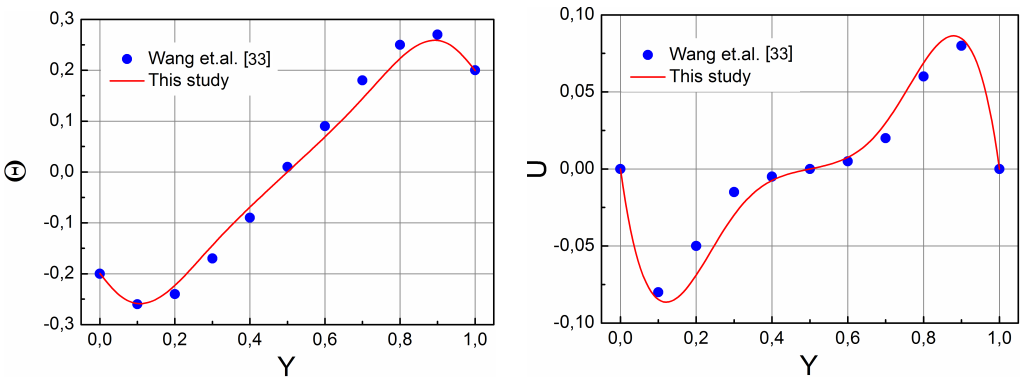


Figure 5: Temperature (a) and velocity (b) distributions when $Ra=10^6$ and $\varepsilon=0.2$.

### 3.1 Effect of $Ra$

Thermal and flow fields with variation of buoyancy force are shown in Fig. 6. The isotherms step is 0.05.

Firstly, it should be stressed that the Rayleigh number variation is directly connected with the conduction-radiation number. A rise in the buoyancy force is concerned with an increment in the characteristic dimension of the cavity. Therefore, the conduction-radiation number is simultaneously increased with the Rayleigh number. When performing a general observation, de-stratification is noticed as the buoyancy force is enhanced. Moreover, turbulent heat transfer and fluid flow patterns associated with a decrease in the boundary layer thickness at the isothermal walls are persisted when taking into account the surface radiation effect. It is found that the thermal and flow behavior is almost insensitive to surface thermal radiation when the $Ra=10^8$ and $N_r=75.89$. A large-eddy directed clockwise with two inner flows near the hot and cold walls is formed as in the case of pure natural convection. However, a slight change in the isotherms shape near the heat-insulated walls is revealed. When rising the $Ra$ and $N_r$ to $10^9$ and 163.45, correspondingly, the surface radiation significantly affects the thermal and flow behavior. Convective plumes are formed not only at the isothermal walls as in the case of pure convection, but this phenomenon is also observed at the heat-insulated boundaries. This factor is obviously concerned with the heating/cooling of the bottom/top wall by irradiation. Along with that, the number of inner flows inside the main convective cell is increased due to the enhancement of both the buoyancy force and the surface radiation. When the $Ra=10^{10}$ and $N_r=351.75$, the thermal field and the flow pattern are drastically altered. Thermal stratification remains in a small area of the analysis domain and a chaotic behavior is observed near the heat-insulated walls due to the high formation rate of the convective plumes. Apparently, this rate determines the level of de-stratification. It is interesting to note that the shape of the main vortex and the location of the inner currents are insignificantly altered. However, the number of small eddies is noticeably increased. Fig. 7 presents distributions of the temperature and the velocity in the characteristic sections.

When analyzing the data presented in Fig. 6, it is revealed that the temperature is insignificantly varied in the section of $Y=0.5$ in a range of $10^8 \leq Ra \leq 10^9$. The highest change is observed near the hot and cold walls since the boundary layer is drastically decreased with a rise in the Rayleigh number. On the other hand, light temperature fluctuations are found both in the sections of $X=0.5$ and $Y=0.5$ with the $Ra=10^{10}$. Moreover, surface radiation contributes to the creation of a steep temperature gradient near the heat-insulated walls with this value of the Rayleigh number. It should be noted that the buoyancy force enhancement reduces the temperature near the top walls whereas a rise in the temperature is observed near the bottom wall. Along with that, the absolute value of the horizontal velocity component along the $X$-axis is increased. On the contrary, the maximum absolute value of $V$ is achieved with the $Ra=10^9$. Probably, surface radiation reduces the speed of the flow along the $Y$-axis due to a decrease in the vertical

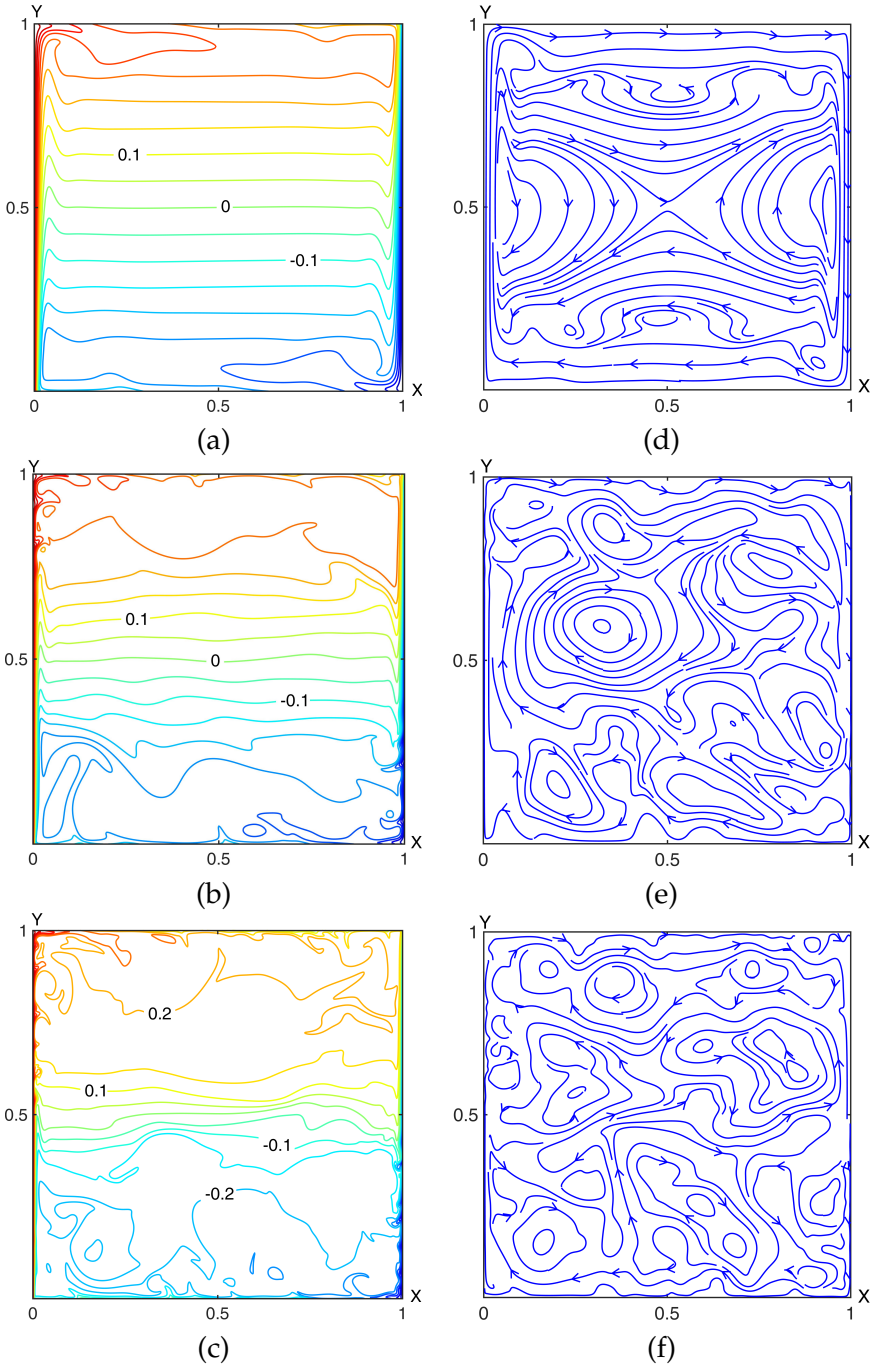


Figure 6: Isotherms (a), (b), (c) and streamslices (d), (e), (f) when $\varepsilon = 0.9$: (a), (d) $\tau = 1500$, $Ra = 10^8$ and $N_r = 75.89$; (b), (e) $\tau = 1000$, $Ra = 10^9$ and $N_r = 163.45$; (c), (f) $\tau = 500$, $Ra = 10^{10}$ and $N_r = 351.75$.

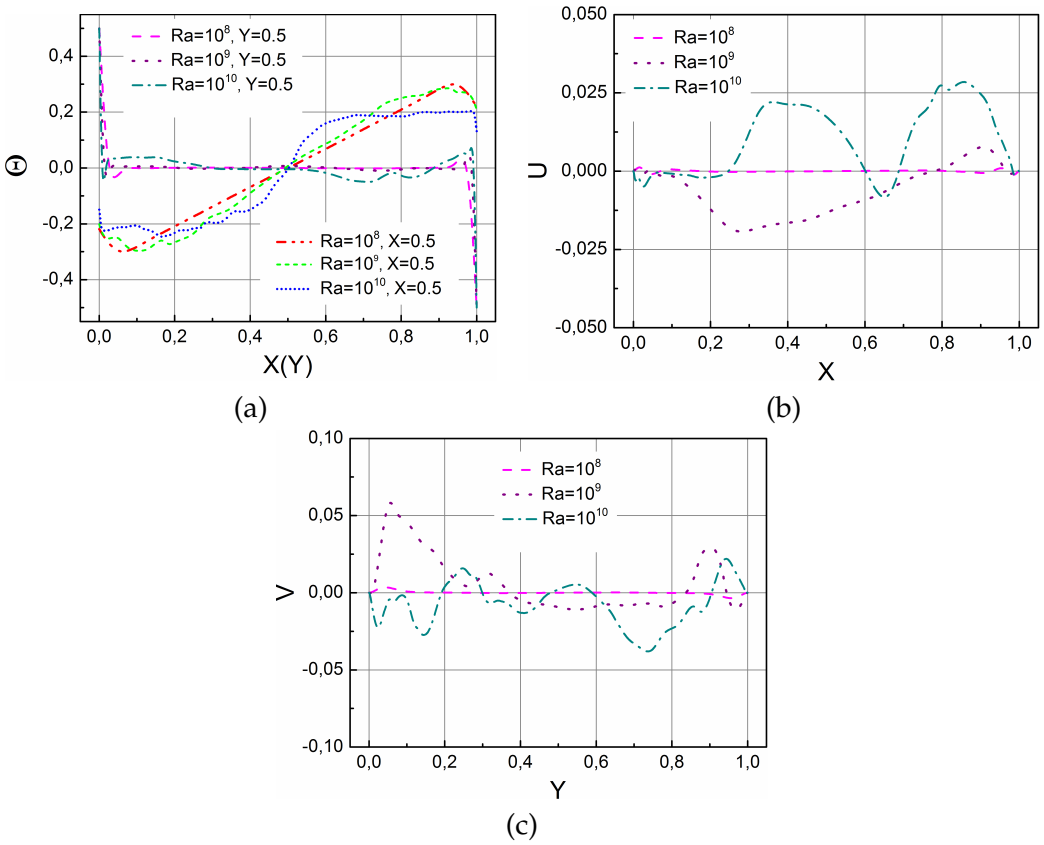


Figure 7: Profiles of temperature (a) and velocity components (b), (c) when $\varepsilon=0.9$: (a) $X=0.5$ and $Y=0.5$; (b) $Y=0.5$; (c) $X=0.5$.

temperature gradient.

## 3.2 The effect of $\varepsilon$

Fig. 8 presents variation of thermal and flow patterns with the emissivity of the walls.

Based on the analysis of the illustrations, it is found that the thermal radiation slightly affects the heat transfer and fluid flow patterns with the $\varepsilon \leq 0.2$. Thermal stratification fills almost the entire cavity and two outer flows are formed at the top left and bottom right corners as in the case of pure turbulent natural convection. When raising the surface emissivity to 0.6, the core of the cavity remains unchanged. However, temperature oscillations appear near the heat-insulated walls. Along with that, the outer flow at the top left corner is expelled whereas an additional eddy outside the main vortex is formed at the bottom left corner. Moreover, more eddies are formed inside the main convective cell as the surface radiation is enhanced. When $\varepsilon=1$, irradiation strongly affects the thermal field. The overall temperature of the solution domain is noticeably increased. On the one

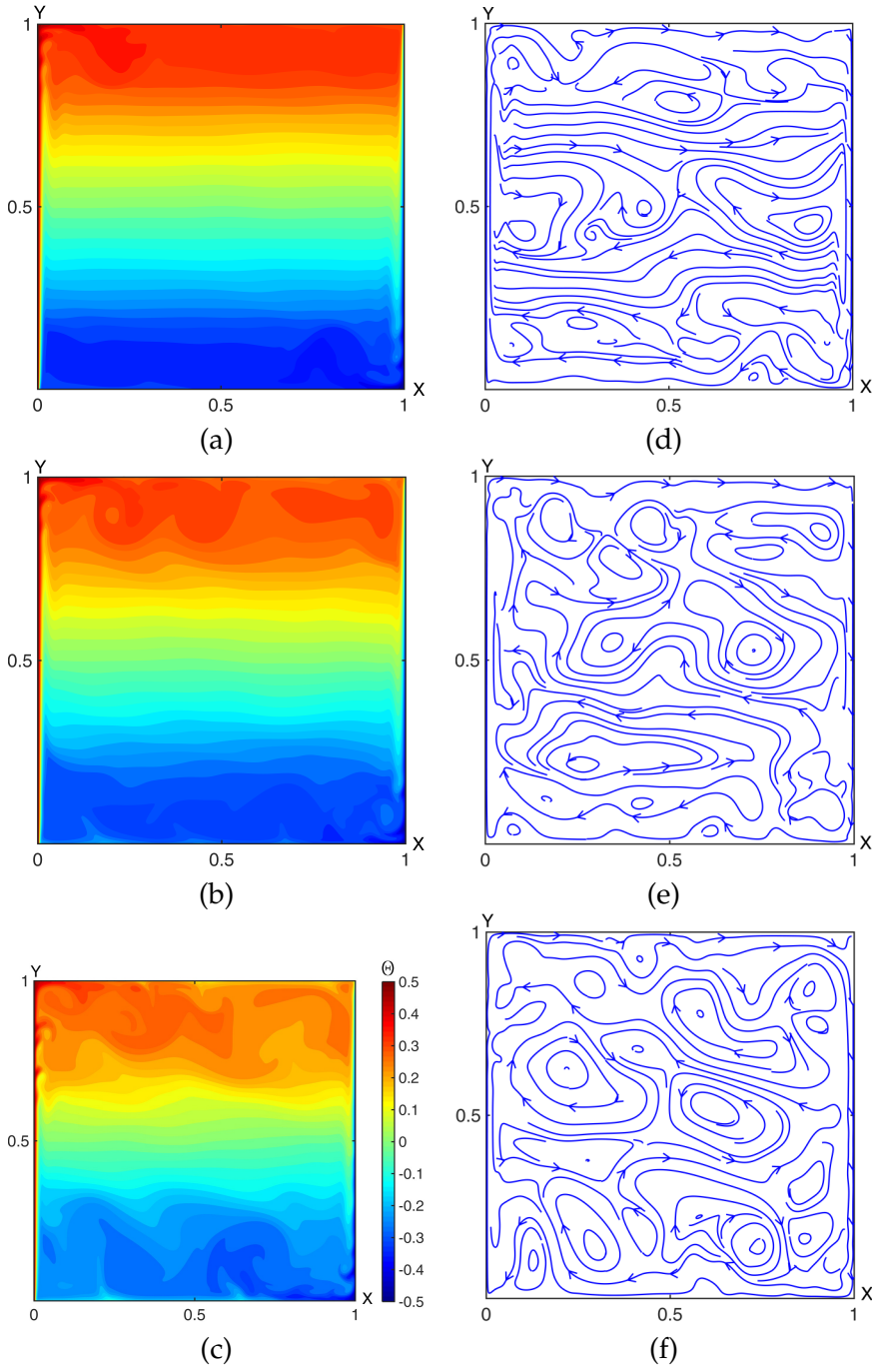


Figure 8: Temperature contours (a), (b), (c) and streamslices (d), (e), (f) when $\tau = 600$, $Ra = 10^9$ and $N_r = 163.45$: (a), (d) $\varepsilon = 0.2$; (b), (e) $\varepsilon = 0.6$; (c), (f) $\varepsilon = 1$.

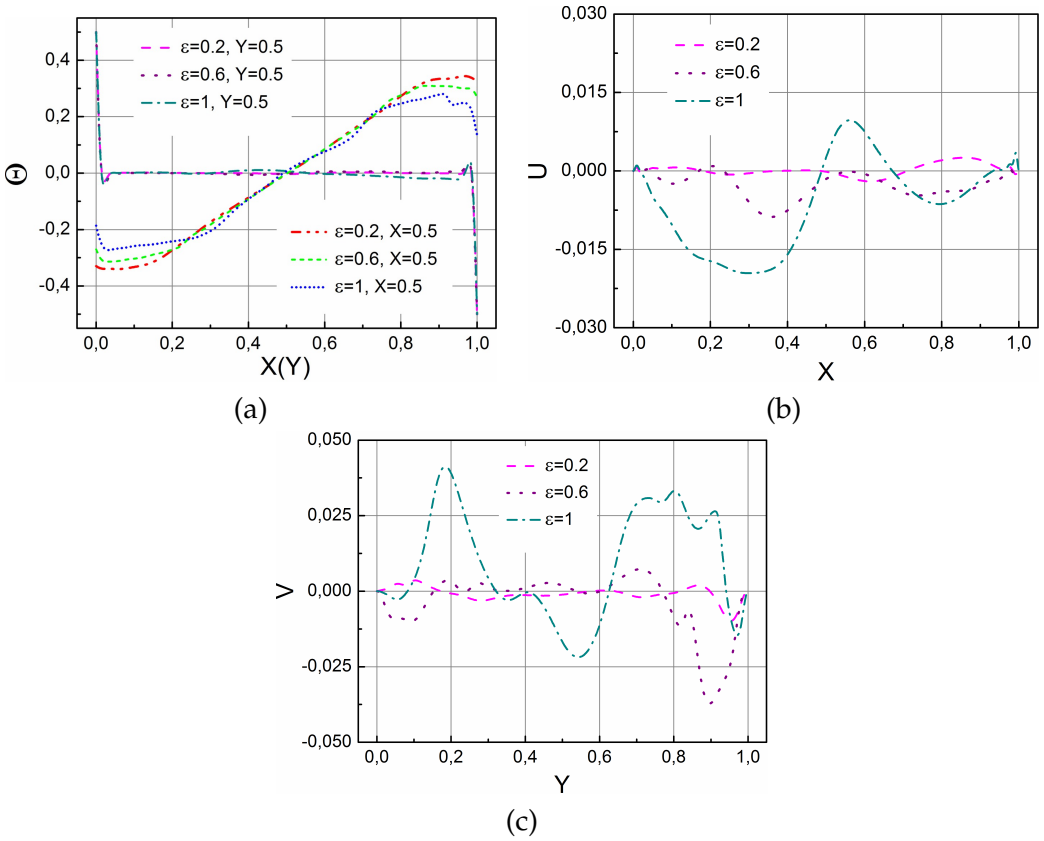


Figure 9: Variation of temperature (a) and velocity components (b), (c) when $Ra=10^9$ and $N_r=163.45$: (a) $X=0.5$ and $Y=0.5$; (b) $Y=0.5$; (c) $X=0.5$.

hand, the net fluxes significantly heat/cool the bottom/top wall. As a result, convective plumes directed upward and downward are formed both at the isothermal and heat-insulated walls. On the other hand, the turbulent mixing rate of the fluid is enhanced due to these phenomena. It should be stressed that this behavior cannot be revealed by the wide-spread RANS models since the high production rate of turbulent viscosity suppresses the light fluctuations of flow. This peculiarity prevents the development of secondary flows and convective plumes. On the contrary, the hybrid TRTLB-FD model proposed in this study successfully deals with this phenomenon. The high formation rate of the convective plumes contributes to the expansion of the outer flow at the bottom left corner. However, the flow pattern in the upper half of the solution domain is modified insignificantly. The temperature and velocity profiles in the medium sections are shown in Fig. 9.

It is found that the temperature distribution near the hot and cold walls is insensitive to the variation of the surface emissivity. Moreover, the temperature profiles are identical

in a range of $0.2 \leq \varepsilon \leq 0.6$ in the section of $Y=0.5$. A slight change in the temperature is only observed with the surface emissivity equals to unity. On the other hand, the surface thermal radiation is seen to significantly affect the temperature near the heat-insulated walls. The temperature of the top wall is decreased whereas the temperature of the bottom wall is increased with the enhancement of the irradiation. In addition, the temperature gradient near the heat-insulated walls is raised. However, the temperature at the core of the cavity barely changes with the $\varepsilon$. When analyzing the velocity profiles, it is revealed that the surface radiation increases the fluid speed in the characteristic sections. Probably, this pattern is concerned with the formation of convective plumes at the heat-insulated boundaries.

### 3.3 Rate of heat transfer

In the present study, the mean Nusselt numbers are assessed to find out how the thermal radiation affects the convective and overall heat transfer rate. The mean convective ($Nu$), radiative ($Nu_R$) and effective ($Nu_E$) Nusselt numbers at the hot wall are computed as:

$$
\begin{aligned}
Nu &= \int_0^L \left.\frac{\partial \Theta}{\partial X}\right|_{X=0} dY, \\
Nu_R &= \int_0^L \left.(Q_{irr} \cdot N_r)\right|_{X=0} dY, \\
Nu_E &= Nu_C + Nu_R.
\end{aligned}
$$

Fig. 10 shows the Nusselt numbers under studied conditions.

When performing an integral analysis, it is found that the heat transfer rate by natural convection is weakened with an increment in the emissivity of the surfaces. However, this decline in the convective Nusselt number is barely noticeable with the $Ra=10^8$ and is enhanced with a rise in the force of buoyancy. Apparently, additional radiant heating and cooling of the bottom and top boundaries reduces the temperature gradient near the hot wall. Since a strong effect of thermal radiation on turbulent natural convection is observed with the highest value of the Rayleigh number, a considerable drop in the $Nu_C$ is revealed with the $Ra=10^{10}$. On the contrary, the radiative Nusselt number is almost linearly grown with changes in the value of the $\varepsilon$. However, this pattern is predictable since the irradiation and surface emissivity are directly proportional quantities. Moreover, the value of $Nu_R$ is increased as the $Ra$ value is risen due to an increment in the conduction-radiation number. When analyzing the overall heat transfer rate, it is discovered that a weakening in the natural convection is counter balanced by the radiative heat transfer. In addition, the effective Nusselt number is approximately increased by 5% in a range of $10^8 \leq Ra \leq 10^{10}$ and $0 \leq \varepsilon \leq 1$.

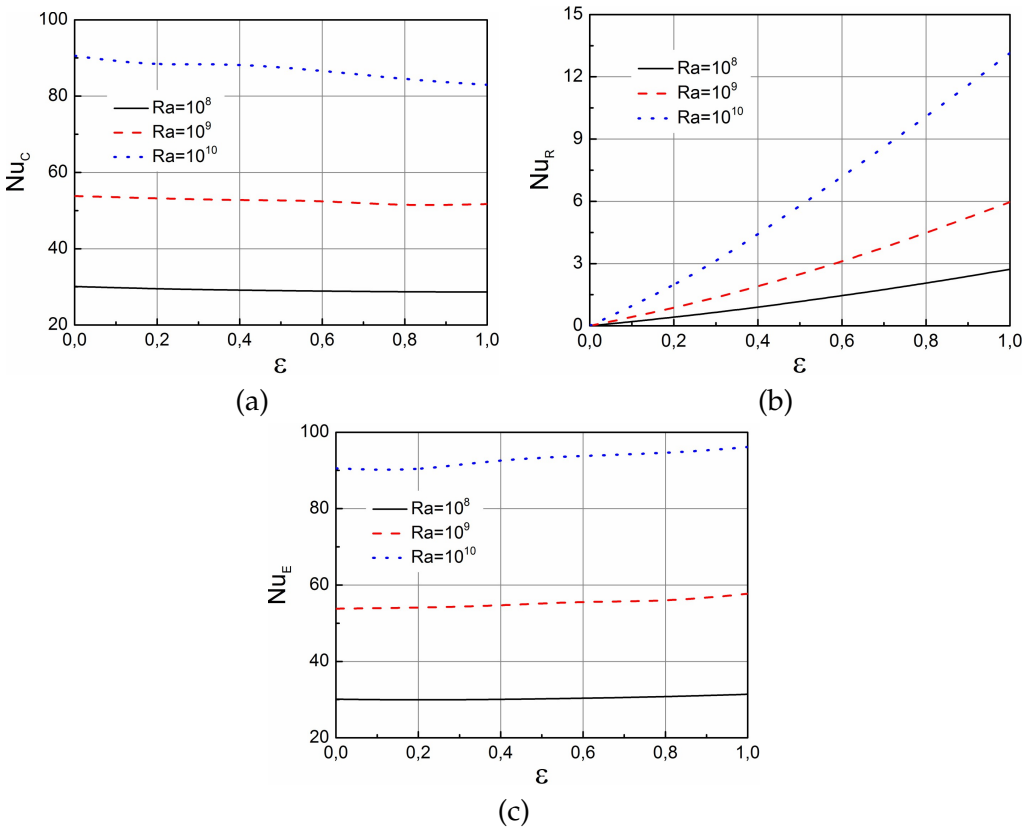


Figure 10: The mean Nusselt numbers variation with the walls emissivity.

## 4 Conclusions

The hybrid two-relaxation time lattice Boltzmann–finite difference solver was built to study the turbulent buoyancy-driven flow coupled with the radiation. The overall robustness of the proposed method was demonstrated in the validation section. When analyzing the interaction of turbulent free convection and surface radiation, the following specific results were obtained:

- The effect of thermal radiation on turbulent free convection becomes stronger with a rise in the buoyancy force. Convective plumes formed at the heat-insulated walls due to the irradiation contribute to the thermal de-stratification. Along with that, the inner convective cells are divided into small eddies. A steep temperature gradient is observed near the top and bottom boundaries with the $Ra = 10^{10}$.
- The overall temperature of the solution domain is increased with an increment in the emissivity of the walls. The temperature at the core of the solution domain and near the isothermal walls is insensitive to the surface emissivity variation. On

the other hand, the temperature of the top boundary is decremented whereas the temperature of the bottom boundary is grown with an increase in the value of the $\varepsilon$. Along with that, an increase in the temperature gradient is observed near the heat-insulated walls.

- When raising the emissivity of the walls, the natural convective heat transfer rate is reduced. Moreover, this reduction gets stronger as the value of the buoyancy force is increased. However, the weakening of the natural convection is counter balanced by the surface radiation. Thus, the total heat transfer rate was increased by around 5%.

In prospect, the coupling of the lattice Boltzmann method with an explicit finite-difference scheme for an advection/diffusion equation is of great importance in terms of the parallel implementation. Along with that, a three-dimensional problem formulation and coupling turbulent convective-radiative heat transfer with the conduction in the enclosure are of interest.

## Nomenclature

| | |
|---|---|
| $a$ | Heat diffusivity, $\mathrm{m}^2/\mathrm{s}$; |
| $c_k$ | Speed of particle, $\mathrm{m}/\mathrm{s}$; |
| $c_s$ | Lattice speed of sound, $\mathrm{m}/\mathrm{s}$; |
| $f$ | Distribution function, $\mathrm{kg}/\mathrm{m}^3$; |
| $g$ | Acceleration due to gravity, $\mathrm{m}/\mathrm{s}^2$; |
| $t$ | Time, s; |
| $t_0$ | Scale of time, s; |
| $\Delta t$ | Lattice time step; |
| $u,v$ | Velocity components, $\mathrm{m}/\mathrm{s}$; |
| $U,V$ | Dimensionless velocity components; |
| $V_{nc}$ | Scale of velocity, $\mathrm{m}/\mathrm{s}$; |
| $x,y$ | Rectangular coordinates, m; |
| $X,Y$ | Dimensionless rectangular coordinates; |
| $T$ | Temperature, K; |
| $\beta$ | Volumetric heat expansion coefficient, $\mathrm{K}^{-1}$; |
| $\varepsilon$ | Emissivity of the walls; |
| $\varphi$ | View factor; |
| $\Lambda$ | Magic parameter; |

| | |
|---|---|
| $\Theta$ | Dimensionless temperature; |
| $\lambda$ | Thermal conductivity, $W/(m\cdot K)$; |
| $\nu$ | Kinematic viscosity, $m^2/s$; |
| $\rho$ | Density, $kg/m^3$; |
| $\sigma$ | Stefan-Boltzmann number, $W/(m^2\cdot K^4)$; |
| $\tau$ | Dimensionless time; |
| 0 | initial state; |
| $c$ | cold wall; |
| $h$ | hot wall. |

## Acknowledgements

The research was carried out within the framework of Tomsk Polytechnic University Development Program.

## References

[1] A. ABIDI, L. KOLSI, M. N. BORJINI, AND H. BEN AISSIA, *Effect of radiative heat transfer on three-dimensional double diffusive natural convection,* Numer. Heat Tr. A-Appl., 60 (2011), pp. 785–809.

[2] A. K. SHARMA, K. VELUSAMY, C. BALAJI, AND S. P. VENKATESHAN, *Conjugate turbulent natural convection with surface radiation in air filled rectangular enclosures,* Int. J. Heat Mass Transf., 50 (2007), pp. 625–639.

[3] A. K. SHARMA, K. VELUSAMY, AND C. BALAJI, *Interaction of turbulent natural convection and surface thermal radiation in inclined square enclosures,* Heat Mass Transfer, 44 (2008), pp. 1153–1170.

[4] D. IYI , R. HASAN, AND R. PENLINGTON, *Effect of emissivity on the heat and mass transfer of humid air in a cavity filled with solid obstacles,* Numer. Heat Tr. A-Appl., 67 (2015), pp. 531–546.

[5] Y. C. WANG, J. YANG, Y. PAN, X. J. ZHANG, AND Y. F. YU, *Turbulent natural convection heat transfer with thermal radiation in a rectangular enclosure partially filled with porous medium,* Numer. Heat Tr. A-Appl., 70 (2016), pp. 639–649.

[6] M. K. DASH, AND S. K. DASH, *Combined effect of turbulent natural convection and radiation from a horizontal cylinder,* J. Thermophys. Heat. Trans., 34 (2020), pp. 1–10.

[7] M. PARMANANDA, R. THIRUMALAISAMY, A. DALAL, AND G. NATARAJAN, *Investigations of turbulence-radiation interaction in non-Oberbeck-Boussinesq buoyancy-driven flows,* Int. J. Therm. Sci., 134 (2018), pp. 298–316.

[8] J. XAMÁN, G. ÁLVAREZ, J. HINOJOSA, AND J. FLORES, *Conjugate turbulent heat transfer in a square cavity with a solar control coating deposited to a vertical semitransparent wall,* Int. J. Heat Fluid Flow, 30 (2009), pp. 237–248.

[9] Y. OLAZO-GOMEZ, J. XAMAN, M. GIJON-RIVERA, F. NOH-PAT, E. SIMA, AND Y. CHAVEZ, *Mathematical modelling of conjugate laminar and turbulent heat transfer in a cavity: Effect of a vertical glazed wall,* Int. J. Therm. Sci., 152 (2020), 106310.

[10] I. V. MIROSHNICHENKO, AND M. A. SHEREMET, *Radiation effect on conjugate turbulent natural convection in a cavity with a discrete heater,* Appl. Math. Comput., 321 (2018), pp. 358–371.
[11] I. V. MIROSHNICHENKO, AND M. A. SHEREMET, *Turbulent natural convection combined with thermal surface radiation inside an inclined cavity having local heater,* Int. J. Therm. Sci., 124 (2018), pp. 122–130.
[12] B. ZAMORA, AND A. S. KAISER, *Radiative and variable thermophysical properties effects on turbulent convective flows in cavities with thermal passive configuration,* Int. J. Heat Mass Transf., 109 (2017), pp. 981–996.
[13] B. ZAMORA, AND A. S. KAISER, *Influence of the shape, thermal radiation, and variable properties on the turbulent buoyancy-driven airflow inside cavities with Trombe wall geometry,* Numer. Heat Tr. A-Appl., 73 (2018), pp. 307–331.
[14] B. ZAMORA, *Heating intensity and radiative effects on turbulent buoyancy-driven airflow in open square cavities with a heated immersed body,* Int. J. Therm. Sci., 126 (2018), pp. 218–237.
[15] C. HEMMER, F. CONVERT, C. POPA, AND G. POLIDORI, *3-D Simulations of indoor airflow and temperature field with a radiative and convective heater,* J. Appl. Fluid Mech., 9 (2016), pp. 189–195.
[16] N. BENYAHIA, M. AKSOUH, A. MATAOUI, AND H. F. OZTOP, *Coupling turbulent natural convection-radiation-conduction in differentially heated cavity with high aspect ratio,* Int. J. Therm. Sci., 158 (2020), 106518.
[17] A. FRANK, W. HEIDEMANN, AND K. SPINDLER, *Electronic component cooling inside switch cabinets: combined radiation and natural convection heat transfer,* Heat and Mass Transfer, 55 (2019), pp. 699–709.
[18] T. WU, AND CH. LEI, *On numerical modelling of conjugate turbulent natural convection and radiation in a differentially heated cavity,* Int. J. Heat Mass Transf., (2015), pp. 454–466.
[19] N. A. A. QASEM, B. IMTEYAZ, R. BEN-MANSOUR, AND M. A. HABIB, *Effect of radiation heat transfer on naturally driven flow through parallel-plate vertical channel,* Arab. J. Sci. Eng., 42 (2017), pp. 1817–1829.
[20] J. M. A. NAVARRO, J. F. HINOJOSA, AND I. HERNANDEZ-LOPEZ, *Computational fluid dynamics and experimental study of turbulent natural convection with surface thermal radiation in a cubic enclosure,* Int. J. Mod. Phys. C, 31 (2020), 2050065
[21] T. KOGAWA, J. OKAJIMA, A. SAKURAI, A. KOMIYA, AND SH. MARUYAMA, *Influence of radiation effect on turbulent natural convection in cubic cavity at normal temperature atmospheric gas,* Int. J. Heat Mass Transf., 104 (2017), pp. 456–466.
[22] SH. XIN, J. SALAT, P. JOUBERT, A. SERGENT, F. PENOT, AND P. LE QUÉRÉ, *Resolving the stratification discrepancy of turbulent natural convection in differentially heated air-filled cavities, Part III: A full convection-conduction-surface radiation coupling,* Int. J. Heat Fluid Flow, 42 (2013), pp. 33–48.
[23] G. BARAKOS, E. MITSOULIS AND D. ASSIMACOPOULOS, *Natural convection flow in a square cavity revisited: Laminar and turbulent models with wall functions,* Int. J. Numer. Methods Fluids, 18 (1994), pp. 695–719.
[24] YA. ADDAD, I. ZAIDI, AND D. LAURENCE, *Quasi-DNS of natural convection flow in a cylindrical annuli with an optimal polyhedral mesh refinement,* Comput Fluids, 118 (2015), pp. 44–52.
[25] E. M. J. KOMEN, L. H. CAMILO, A. SHAMS, B. J. GEURTS, AND B. KOREN, *A quantification method for numerical dissipation in quasi-DNS and under-resolved DNS, and effects of numerical dissipation in quasi-DNS and under-resolved DNS of turbulent channel flows,* J. Comput. Phys., 345 (2017), pp. 565–595.
[26] A. K. HUSSEIN, H. R. ASHORYNEJAD, S. SIVASANKARAN, L. KOLSI, M. SHIKHOLESLAMI,

AND I. K. ADEGUN, *Modeling of MHD natural convection in a square enclosure having an adiabatic square shaped body using lattice Boltzmann method,* Alex End. J., 55 (2016), pp. 203–214.

[27] I. GINZBURG, F. VERHAEGHE, AND D. D'HUMIERES, *Study of simple hydrodynamic solutions with the two-relaxation-times lattice Boltzmann scheme,* Commun. Comput. Phys., 3 (2008), pp. 519–584.

[28] W. ZHAO, L. WANG, AND W.-A. YONG, *On a two-relaxation-time D2Q9 lattice Boltzmann model for the Navier-Stokes equations,* Phys. A, 492 (2018), pp. 1570–1580.

[29] J. A. ESFAHANI, AND A. NOROUZI, *Two relaxation time lattice Boltzmann model for rarefied gas flows,* Phys. A, 393 (2014), pp. 51–61.

[30] Y. GUAN, AND I. NOVOSSELOV, *Two relaxation time lattice Boltzmann method coupled to fast Fourier transform Poisson solver: Application to electroconvective flow,* J. Comput. Phys., 397 (2019), 108830.

[31] YO.-L. FENG, SH.-L. GUO, W.-Q. TAO AND P. SAGAUT, *Regularized thermal lattice Boltzmann method for natural convection with large temperature differences,* Int. J. Heat Mass Transf., 125 (2018), pp. 1379–1391.

[32] M. R. SALIMI, E. ALIZADEH-SERESHT, AND M. TAEIBI-RAHNI, *New hybrid finite volume-thermal lattice Boltzmann method, based on multi relaxation time collision operator,* Int. J Heat Mass Transf., 138 (2019), pp. 1281–1294.

[33] CH. OBRECHT, F. KUZNIK, B. TOURANCHEAU, AND J.-J. ROUX, *Multi-GPU implementation of a hybrid thermal lattice Boltzmann solver using the TheLMA framework,* Comput. Fluids, 80 (2013), pp. 269–275.

[34] G. V. KUZNETSOV, N. I. KURILENKO, AND A. E. NEE, *Mathematical modelling of conjugate heat transfer and fluid flow inside a domain with a radiant heating system,* Int. J. Therm. Sci., 131 (2018), pp. 27–39.

[35] A. NEE, *Hybrid lattice Boltzmann–Finite difference formulation for combined heat transfer problems by 3D natural convection and surface thermal radiation,* Int. J. Mech. Sci., 173 (2020), 105447.

[36] K. V. SHARMA, R. STRAKA, AND F. W. TAVARES, *Natural convection heat transfer modeling by the cascaded thermal lattice Boltzmann method,* Int. J. Therm. Sci., 134 (2018), pp. 552–564.

[37] F. AMPOFO, AND T. G. KARAYIANNIS, *Experimental benchmark data for turbulent natural convection in an air filled square cavity,* Int. J. Heat Mass. Transf., 46 (2003), pp. 3551–3572.

[38] H. WANG, S. XIN, AND P. LE QUERE, *Numerical study of natural convection-surface radiation coupling in air-filled square cavities,* Comptes Rendus Mecanique, 334 (2006), pp. 48–57.